Supporting Information

Experimental section

Chemicals and materials

Cobalt oxide (AR) and sodium hydroxide (AR, 96%) were supplied by Aladdin. Palladium (II) chloride (Pd: 59.86%) was purchased from Kunming Boren Precious Metals Co., Ltd. Sodium chloride (AR) and sodium borohydride (AR) were supplied by Ke Long chemical Reagent Factory. Borane-ammonia complex (97%) was purchased from Innochem. All the reagents were used as received without further purification.

Characterization

Transmission electron microscopy (TEM) with a JEOL JEM-2100F (JEOL) was used to characterize the morphology and particle size of samples. The crystal structure for samples were detected by X-ray diffraction (XRD) on a Regaku D/XMax-2500 diffractometer under Cu Kα radiation. X-ray photoelectron spectroscopy (XPS) was used to determine the composition and valence states of samples on a Thermo ESCALAB 250 Axis Ultra spectrometer. N_2 sorption measurement was carried out on a Micromeritics ASAP 2460 and Brunauer–Emmett–Teller (BET) method was used to calculate the surface area of samples. The Pd loadings of the catalysts were measured via inductively coupled plasma optical emission spectrometry (ICP-OES, PerkinElmer Optima 8000 equipment).

Computational Method

Equation S1 Calculation formula of TOF values.

$$TOF = \frac{n(H_2)}{n(Pd)t} \quad (1)$$

where n (H_2) is 40% of the total hydrogen moles of the AB generated hydrogen, n (Pd) is the number of moles in Pd/Co_3O_4-SB, and t is the corresponding n (H_2) time.

According the method reported by Qing-Yuan Bi et al [1] (Equation S2), the Pd dispersion was calculated based on an assumption of a quasi-hemispherical model of Pd particle. TEM image showed that the average particle size of Pd was 2.11 nm (Fig. 3c). Therefore, the Pd dispersion on the catalyst surface was calculated to be 62%. In general, an error of ±10% was established for the results.

Equation S2 Calculation formula of Pd dispersion.

$$Dispersion = \frac{N_S}{N_T} = \frac{Sk}{n_{Pd}N_A} \quad (2)$$

The overall surface area of Pd particles: $S = 2\pi(\frac{d_{Pd}}{2})^2 N_1$

The number of Pd particles: $N_1 = \frac{m_{Pd}}{\frac{2}{3}\pi(\frac{d_{Pd}}{2})^3 \rho_{Pd}}$

The moles of pd: $n = \frac{m_{Pd}}{M_{Pd}}$

N_S = total number of surfaces Pd atoms

N_T = total number of Pd atoms

The Pd atom density (k) = 1×10^{17} m^{-2}

ρ = 12.02 g cm^{-3} N_A = 6.02*10^{23} mol^{-1} d_{Pd} = 2.11nm

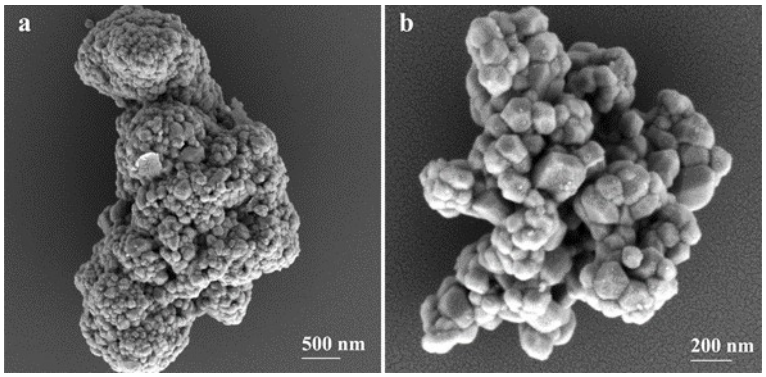

Fig. S1. SEM images of Pd/Co_3O_4-AB.

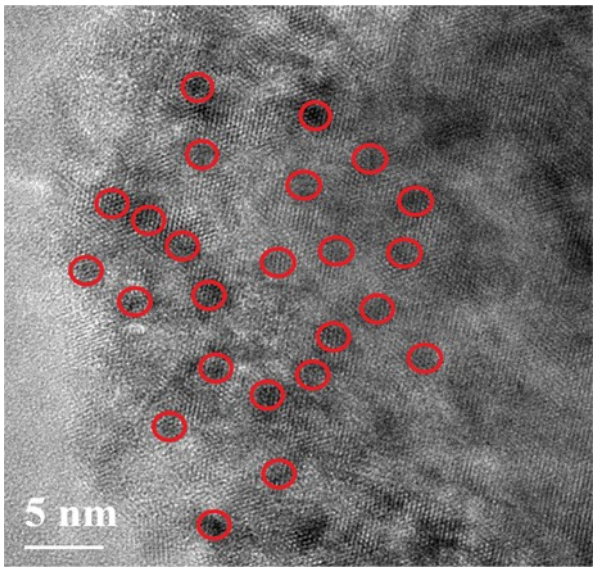

Fig. S2. Representative Pd on the surface of Co_3O_4-SB are highlighted by the red circles.

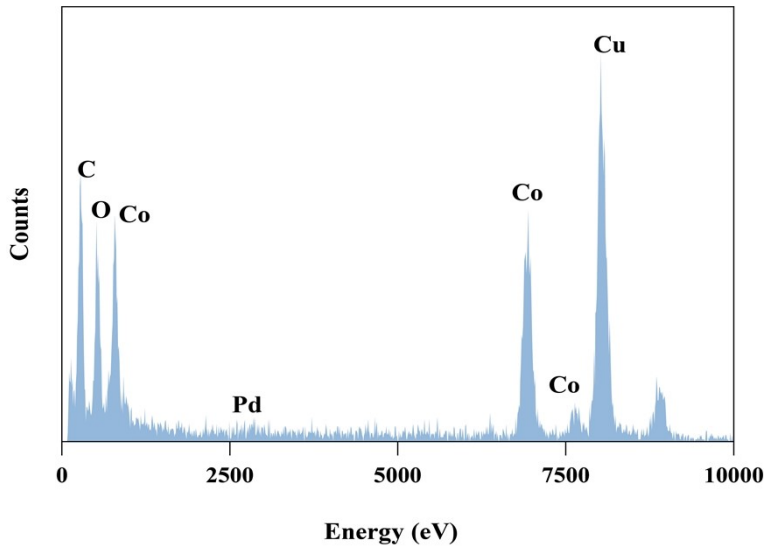

Fig. S3. Energy dispersive spectroscopy (EDS) image of Pd/Co_3O_4-SB.

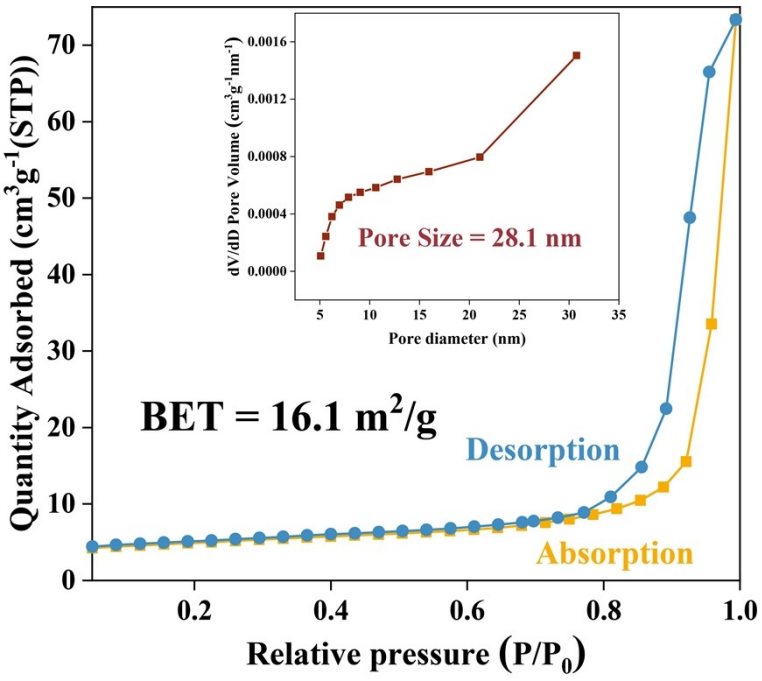

Fig. S4. N_2 adsorption–desorption isotherms and (inset) pore diameter distribution of Co_3O_4-SB.

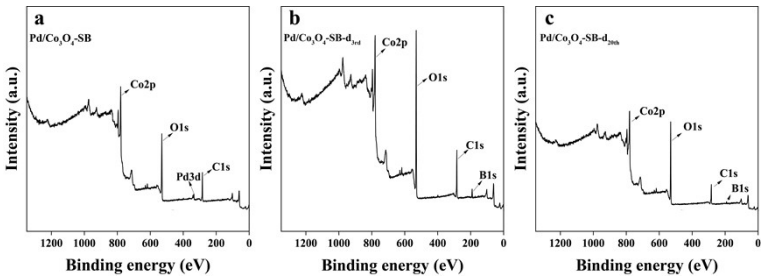

Fig. S5. XPS survey spectra for (a) Pd/Co_3O_4-SB, (b) Pd/Co_3O_4-SB-d_{3rd} and (c) Pd/Co_3O_4-SB-d_{20th}.

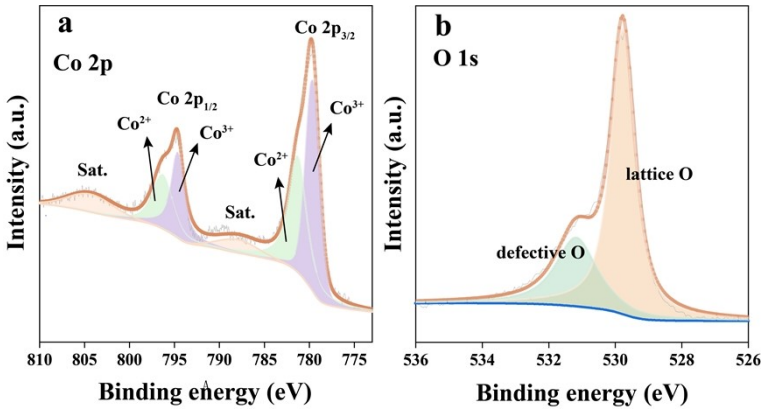

Fig. S6. High-resolution XPS spectra for (a) Co 2p and (b) O 1s of Co_3O_4.

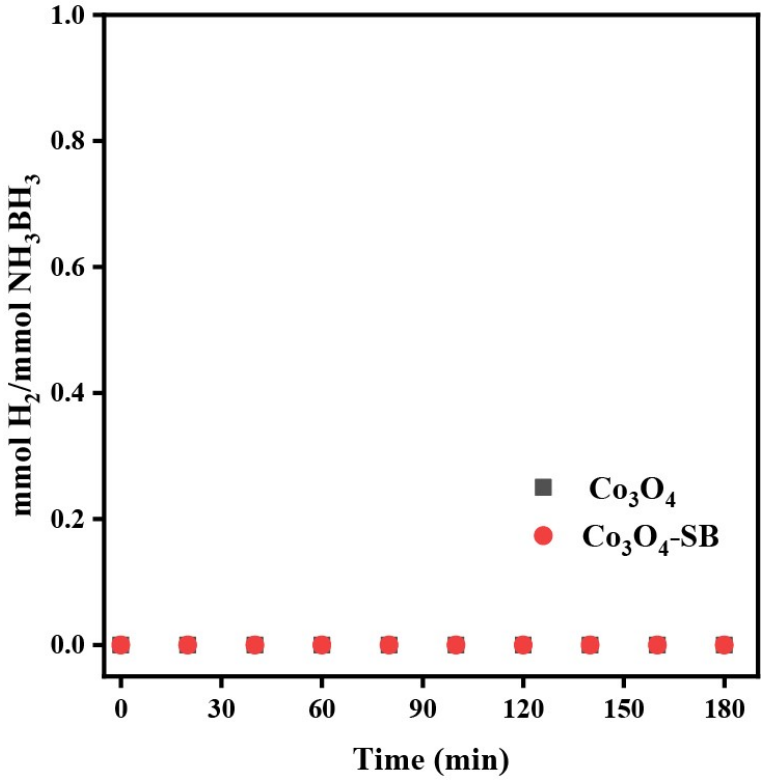

Fig. S7. H_2 evolution curves by catalysts of Co_3O_4 and Co_3O_4-SB.

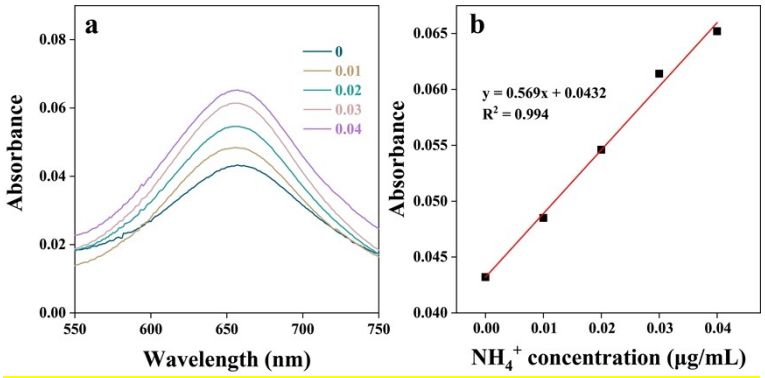

Fig. S8. NH_3 quantification using indophenol blue method. (a) The UV-vis absorption spectra and (b) corresponding calibration curves for a series of standard concentrations of NH^{4+} solution.

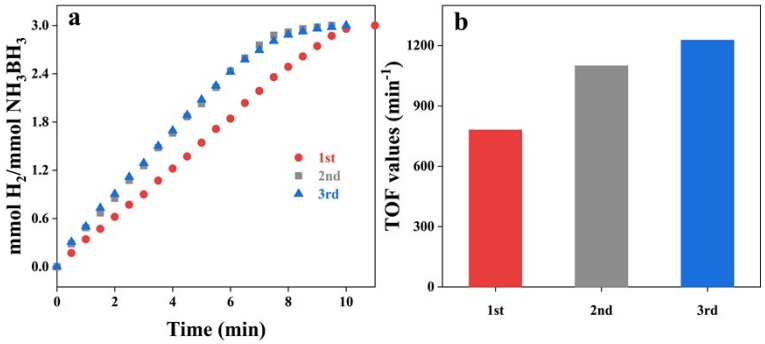

Fig. S9. (a) H_2 evolution curves by the catalysts in durability experiments of 1st (Pd/Co_3O_4-SB), 2rd and the 3rd (Pd/Co_3O_4-SB-d_{3rd}) and (b) the corresponding histogram of TOFs.

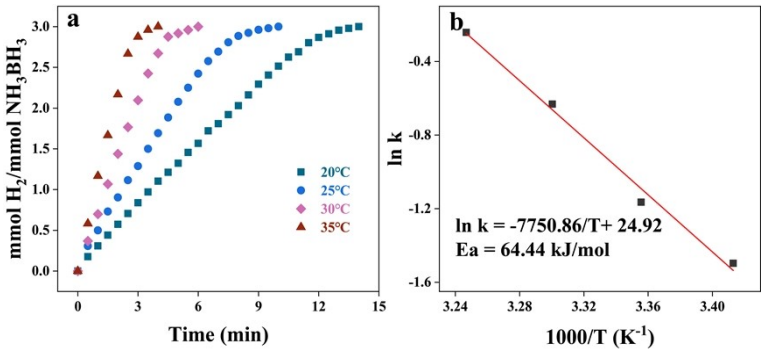

Fig. S10. (a) H_2 evolution curves conducted by Pd/Co_3O_4-SB-d_{3rd} with different temperatures, and (b) the Arrhenius plot.

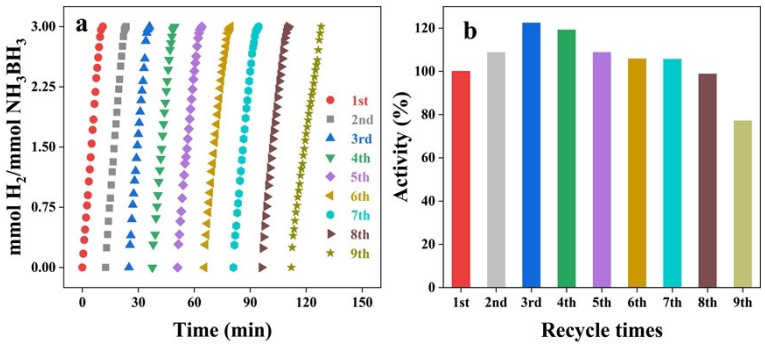

Fig. S11. (a) The reusability tests for AB hydrolysis catalyzed by Pd/Co_3O_4-SB and (b) the corresponding histogram of catalytic activity.

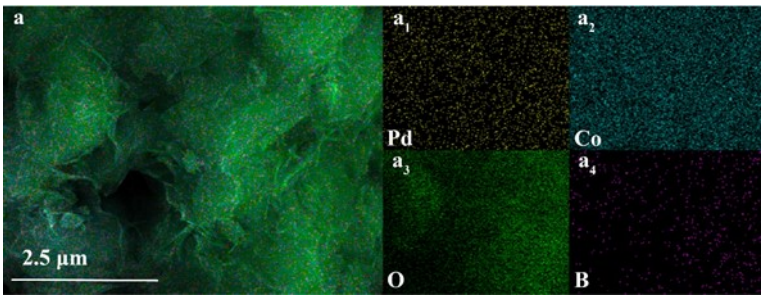

Fig. S12. (a) Elemental mapping of Pd/Co_3O_4-SB-d_{3rd} correspond to (a_1) Pd, (a_2) Co, (a_3) O and (a_4) B maps, respectively.

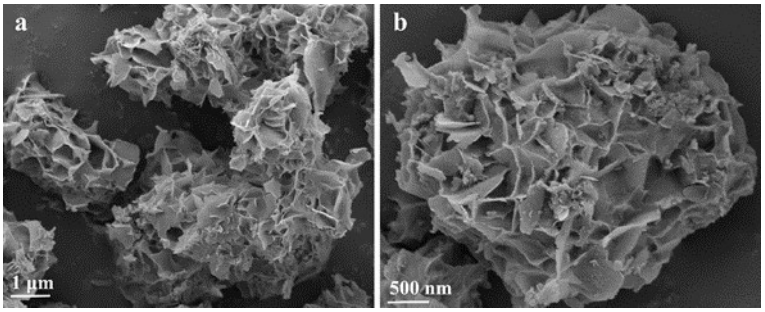

Fig. S13. SEM images of Pd/Co_3O_4-SB-r_{3rd}.

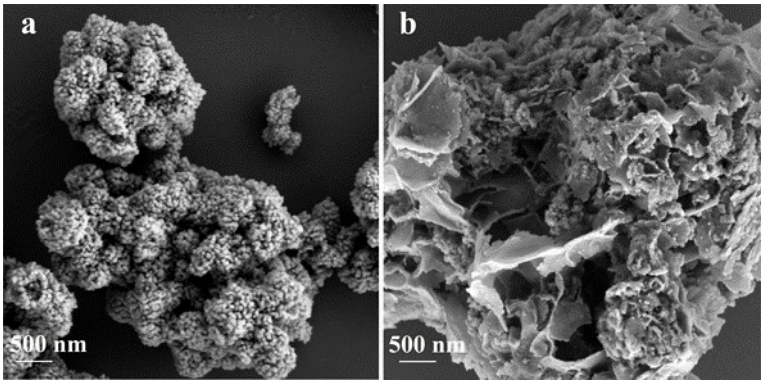

Fig. S14. SEM images of (a) Co_3O_4-SB-d_{3rd} and (b) Pd/Co_3O_4-AB-d_{3rd}.

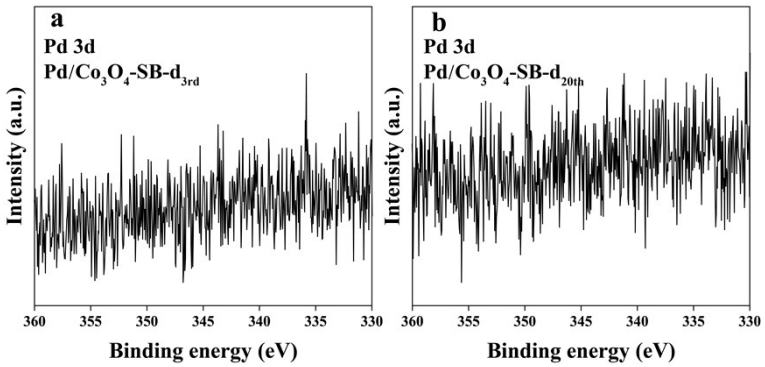

Fig. S15. High-resolution XPS spectra for Pd 3d of (a) Pd/Co_3O_4-SB-d_{3rd} and (b) Pd/Co_3O_4-SB-d_{20th}.

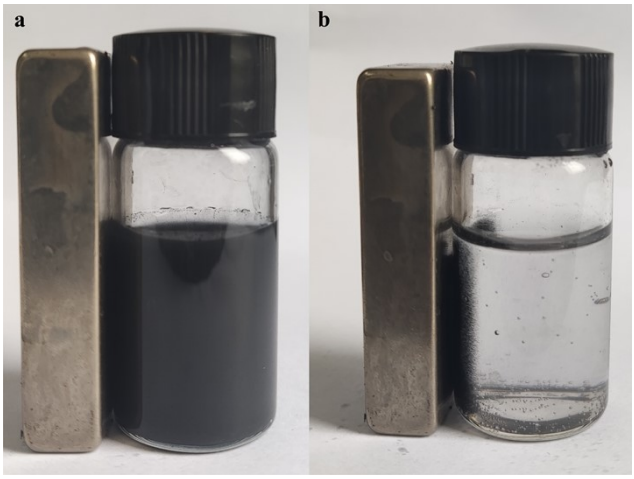

Fig. S16. Photos of the (a) Pd/Co_3O_4-SB and (b) Pd/Co_3O_4-SB-d_{3rd} in the presence of external magnet

Table S1. The Co2p XPS information in Co_3O_4, Pd/Co_3O_4-SB, Pd/Co_3O_4-SB-d_{3rd} and Pd/Co_3O_4-SB-d_{20th}.

Samples	Co^{2+} and Co^{3+} $2p_{3/2}$ peak positions (eV)	Co^{2+}/Co^{3+}
Co_3O_4	781.20 and 779.62	0.908
Pd/Co_3O_4-SB	780. 59 and 779.16	0.926
Pd/Co_3O_4-SB-d_{3rd}	780.88 and 779.67	1.16
Pd/Co_3O_4-SB-d_{20th}	781.57 and 780.11	1.50

Table S2. The O1s XPS information in Co_3O_4, Pd/Co_3O_4-SB, Pd/Co_3O_4-SB-d_{3rd} and Pd/Co_3O_4-SB-d_{20th}.

Samples	lattice oxygen (O_l) and defective oxygen (O_d) peak positions (eV)	O_d/O_l
Co_3O_4	529.70 and 531.20	0.412
Pd/Co_3O_4-SB	529.29 and 530.73	1.21
Pd/Co_3O_4-SB-d_{3rd}	530.18 and 531.15	1.56
Pd/Co_3O_4-SB-d_{20th}	529.98 and 530.90	3.11

Table S3. Comparison results of previous Pd-based catalysts for AB hydrolysis.

Entry	Catalysts	TOF (min^{-1})	Ea (kJ mol^{-1})	Cycles	Remained activity (%)	References
1	RGO/Pd	6.25	51	5	65	[2]
2	Pd/graphene aerogel	9.7	30.82	6	-	[3]
3	Pd^0/PDA–Fe_3O_4	14.5	65	10	100	[4]
4	Pd/PPy	21.1	33.5	5	89	[5]
5	Pd NPs/CS	24.76	32.65	11	-	[6]
6	Pd(0)/GO-ILCS	25.6	38	6	-	[7]
7	RGO@Pd	26.3	40	10	95	[8]
8	Pd/CGP-GO-Fe_3O_4	27.4	36.5	8	-	[9]
9	Pd/Fe_3O_4@SiO_2-PC	28.4	47.3	9	-	[10]
10	Pd^0/CeO_2	29	68	5	47	[11]
11	RGO-$Cu_{75}Pd_{25}$	29.9	45	3	-	[12]
12	Pd@PMOs	30.08	34.9	5	75	[13]
13	Pd NPs/CS-rGO	42.5	39.02	4	-	[14]
14	Pd@MIL-101	45	-	5	-	[15]
15	Pd/α-LDH	49.5	20.56	5	-	[16]
16	mpg-C_3N_4/Pd	66.3	53.6	5	75	[17]
17	Pd/GNS	101.5	46.5	5	74.6	[18]

18	Pd/MCN	125	57	5	-	[19]
19	Pd^0/PDA–$CoFe_2O_4$	175	65	10	100	[20]
20	Ni_3-Pd_7/CS	182	35.32	5	-	[21]
21	Pd(0)/SiO_2–$CoFe_2O_4$	254	52	10	78	[22]
22	Pd_1/Co_3O_4	1470	-	15	100	[23]
23	**Pd/Co_3O_4-SB**	**781**	**61.45**	**20**	**130**	**This work**
24	**Pd/Co_3O_4-SB-d_{3rd}**	**1228**	**64.44**	**-**	**-**	**This work**

References

[1] Bi Q-Y, Du X-L, Liu Y-M, Cao Y, He H-Y, Fan K-N. Efficient Subnanometric Gold-Catalyzed Hydrogen Generation via Formic Acid Decomposition under Ambient Conditions. Journal of the American Chemical Society. 2012;134:8926-33.

[2] Xi PX, Chen FJ, Xie GQ, Ma C, Liu HY, Shao CW, et al. Surfactant free RGO/Pd nanocomposites as highly active heterogeneous catalysts for the hydrolytic dehydrogenation of ammonia borane for chemical hydrogen storage. Nanoscale. 2012;4:5597-601.

[3] Zhong W-d, Tian X-k, Yang C, Zhou Z-x, Liu X-w, Li Y. Active 3D Pd/graphene aerogel catalyst for hydrogen generation from the hydrolysis of ammonia-borane. International Journal of Hydrogen Energy. 2016;41:15225-35.

[4] Manna J, Akbayrak S, Ozkar S. Palladium(0) nanoparticles supported on polydopamine coated Fe3O4 as magnetically isolable, highly active and reusable catalysts for hydrolytic dehydrogenation of ammonia borane. Rsc Advances. 2016;6:102035-42.

[5] Wang Q, Liu Z, Wang W, Liu D, Shi W, He J, et al. Nanostructured palladium/polypyrrole composite paper for enhanced catalytic hydrogen generation from ammonia borane. International Journal of Hydrogen Energy. 2016;41:8470-8.

[6] Chen X, Xu X-J, Zheng X-C, Guan X-X, Liu P. Chitosan supported palladium nanoparticles: The novel catalysts for hydrogen generation from hydrolysis of ammonia borane. Materials Research Bulletin. 2018;103:89-95.

[7] Jia H, Chen X, Liu C-Y, Liu X-J, Zheng X-C, Guan X-X, et al. Ultrafine palladium nanoparticles anchoring graphene oxide-ionic liquid grafted chitosan self-assembled materials: The novel organic-inorganic hybrid catalysts for hydrogen generation in hydrolysis of ammonia borane. International Journal of Hydrogen Energy. 2018;43:12081-90.

[8] Kılıç B, Şencanlı S, Metin Ö. Hydrolytic dehydrogenation of ammonia borane catalyzed by reduced graphene oxide supported monodisperse palladium nanoparticles: High activity and detailed reaction kinetics. Journal of Molecular Catalysis A: Chemical. 2012;361-362:104-10.

[9] Jia H, Liu S, Zheng G-P, Zheng X-C, Wang X-Y, Liu P. Collagen-graphene oxide magnetic hybrids anchoring Pd(0) catalysts for efficient H2 generation from ammonia borane. International Journal of Hydrogen Energy. 2019;44:27022-9.

[10] Liu S, Li Y-T, Zheng X-C, Guan X-X, Zhang X-L, Liu P. Pd nanoparticles anchoring to core-shell Fe3O4@SiO2-porous carbon catalysts for ammonia borane hydrolysis. International Journal of Hydrogen Energy. 2020;45:1671-80.

[11] Tonbul Y, Akbayrak S, Özkar S. Palladium(0) nanoparticles supported on ceria: Highly active and reusable catalyst in hydrogen generation from the hydrolysis of ammonia borane. International Journal of Hydrogen Energy. 2016;41:11154-62.

[12] Güngörmez K, Metin Ö. Composition-controlled catalysis of reduced graphene oxide supported CuPd alloy nanoparticles in the hydrolytic dehydrogenation of ammonia borane. Applied Catalysis A: General. 2015;494:22-8.

[13] Deka JR, Saikia D, Chen P-H, Chen K-T, Kao H-M, Yang Y-C. Palladium nanoparticles encapsulated in carboxylic acid functionalized periodic mesoporous organosilicas as efficient and reusable heterogeneous catalysts for hydrogen generation from ammonia borane. Materials Research Bulletin. 2020;125:110786.

[14] Liu S, Chen X, Wu Z-J, Zheng X-C, Peng Z-K, Liu P. Chitosan-reduced graphene oxide hybrids

encapsulated Pd(0) nanocatalysts for H2 generation from ammonia borane. International Journal of Hydrogen Energy. 2019;44:23610-9.
[15] Dai H, Su J, Hu K, Luo W, Cheng G. Pd nanoparticles supported on MIL-101 as high-performance catalysts for catalytic hydrolysis of ammonia borane. International Journal of Hydrogen Energy. 2014;39:4947-53.
[16] Zhou Y-H, Wang S, Zhang Z, Williams N, Cheng Y, Gu J. Hollow nickel-cobalt layereddouble hydroxide supported palladium catalysts with superior hydrogen evolution activity for hydrolysis of ammonia borane. Chemcatchem. 2018;10:3206-13.
[17] Nisanci B, Turgut M, Sevim M, Metin O. Three-component cascade reaction in a tube: in situ synthesis of Pd nanoparticles supported on mpg-C_3N_4, dehydrogenation of ammonia borane and hydrogenation of nitroarenes. Chemistryselect. 2017;2:6344-9.
[18] Karatas Y, Gulcan M, Celebi M, Zahmakiran M. Pd(0) nanoparticles decorated on graphene nanosheets (GNS): synthesis, definition and testing of the catalytic performance in the methanolysis of ammonia borane at room conditions. Chemistryselect. 2017;2:9628-35.
[19] Wang W, Lu Z-H, Luo Y, Zou A, Yao Q, Chen X. Mesoporous carbon nitride supported Pd and Pd-Ni nanoparticles as highly efficient catalyst for catalytic hydrolysis of NH3BH3. Chemcatchem. 2018;10:1620-6.
[20] Manna J, Akbayrak S, Özkar S. Palladium(0) nanoparticles supported on polydopamine coated CoFe2O4 as highly active, magnetically isolable and reusable catalyst for hydrogen generation from the hydrolysis of ammonia borane. Applied Catalysis B: Environmental. 2017;208:104-15.
[21] Shang N, Zhou X, Feng C, Gao S, Wu Q, Wang C. Synergetic catalysis of NiPd nanoparticles supported on biomass-derived carbon spheres for hydrogen production from ammonia borane at room temperature. International Journal of Hydrogen Energy. 2017;42:5733-40.
[22] Akbayrak S, Kaya M, Volkan M, Özkar S. Palladium(0) nanoparticles supported on silica-coated cobalt ferrite: A highly active, magnetically isolable and reusable catalyst for hydrolytic dehydrogenation of ammonia borane. Applied Catalysis B: Environmental. 2014;147:387-93.
[23] Li J, Guan Q, Wu H, Liu W, Lin Y, Sun Z, et al. Highly active and stable metal single-atom catalysts achieved by strong electronic metal–support interactions. Journal of the American Chemical Society. 2019;141:14515-9.